DNA 5134F

TITANIUM RESPONSE TO A NUCLEAR RADIATION ENVIRONMENT

K. Triebes
Acurex Corporation/Aerotherm
Aerospace Systems Division
485 Clyde Avenue
Mountain View, California 94042

1 November 1979

Final Report for Period 1 January 1979—1 November 1979

CONTRACT No. DNA 001-79-C-0158

APPROVED FOR PUBLIC RELEASE;
DISTRIBUTION UNLIMITED.

THIS WORK SPONSORED BY THE DEFENSE NUCLEAR AGENCY
UNDER RDT&E RMSS CODE B342079464 N99QAXAH12308 H2590D.

Prepared for
Director
DEFENSE NUCLEAR AGENCY
Washington, D. C. 20305

Destroy this report when it is no longer needed. Do not return to sender.

PLEASE NOTIFY THE DEFENSE NUCLEAR AGENCY, ATTN: STTI, WASHINGTON, D.C. 20305, IF YOUR ADDRESS IS INCORRECT, IF YOU WISH TO BE DELETED FROM THE DISTRIBUTION LIST, OR IF THE ADDRESSEE IS NO LONGER EMPLOYED BY YOUR ORGANIZATION.

UNCLASSIFIED

SECURITY CLASSIFICATION OF THIS PAGE (When Data Entered)

REPORT DOCUMENTATION PAGE	READ INSTRUCTIONS BEFORE COMPLETING FORM
1 REPORT NUMBER: DNA 5134F	2 GOVT ACCESSION NO.: A090139
3 RECIPIENT'S CATALOG NUMBER:	
4 TITLE (and Subtitle): TITANIUM RESPONSE TO A NUCLEAR RADIATION ENVIRONMENT	5 TYPE OF REPORT & PERIOD COVERED: Final Report, for Period 1 Jan 79—1 Nov 79.
6 PERFORMING ORG. REPORT NUMBER: FR-79-22-AS, Project 7831	
7 AUTHOR(s): K. Triebes	8 CONTRACT OR GRANT NUMBER(s): DNA 001-79-C-0158 NEW
9 PERFORMING ORGANIZATION NAME AND ADDRESS: Acurex Corporation/Aerotherm, Aerospace Systems Division, 485 Clyde Avenue Mountain View, California 94042	10 PROGRAM ELEMENT, PROJECT, TASK AREA & WORK UNIT NUMBERS: Subtask N99QAXAH123-08
11 CONTROLLING OFFICE NAME AND ADDRESS: Director Defense Nuclear Agency Washington, D.C. 20305	12 REPORT DATE: 1 November 1979
	13 NUMBER OF PAGES: 36
14 MONITORING AGENCY NAME & ADDRESS (if different from Controlling Office)	15 SECURITY CLASS (of this report): UNCLASSIFIED
	15a DECLASSIFICATION DOWNGRADING SCHEDULE

16 DISTRIBUTION STATEMENT (of this Report)

Approved for public release; distribution unlimited.

17 DISTRIBUTION STATEMENT (of the abstract entered in Block 20, if different from Report)

18 SUPPLEMENTARY NOTES

This work sponsored by the Defense Nuclear Agency under RDT&E RMSS Code B342079464 N99QAXAH12308 H2590D.

19 KEY WORDS (Continue on reverse side if necessary and identify by block number)

Titanium Autoignition
Electron Beam Testing
Missile Shroud Vulnerability

20 ABSTRACT (Continue on reverse side if necessary and identify by block number)

Titanium samples were tested in electron beam environments with airflow and sample heating to simulate combined aerodynamic and nuclear effects on missile shrouds. This report describes the pretest analyses, hardware development and the results of the preliminary experiments performed for system checkout. Under conditions which represented mild overtests of potential flight environments, no evidence of sustained combustion was observed in titanium samples.

DD FORM 1 JAN 73 1473 EDITION OF 1 NOV 65 IS OBSOLETE

UNCLASSIFIED

SECURITY CLASSIFICATION OF THIS PAGE (When Data Entered)

410 634

TABLE OF CONTENTS

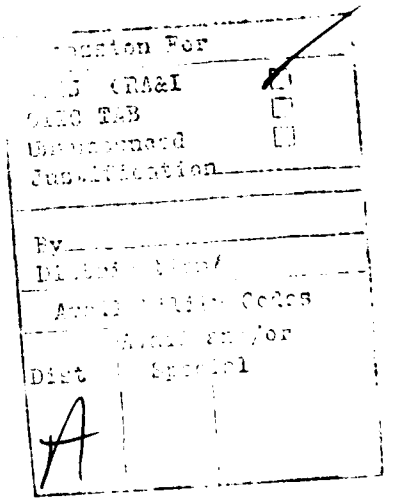

LIST OF ILLUSTRATIONS

SECTION 1

INTRODUCTION

Titanium is a candidate material for advanced missile shrouds. Because titanium may combust under the proper conditions, survivability and vulnerability assessments must be performed to determine the shroud's ability to survive a radiation threat. During the ascent phase of the missile trajectory, shroud ignition may be triggered by two prime mechanisms: (1) dust erosion-induced augmented heating, and (2) an upper atmosphere nuclear encounter. The objective of this program was to investigate the response of titanium to a nuclear environment performing a laboratory scale experiment which simulated the conditions of an upper atmosphere nuclear encounter.

A preliminary analysis of the potential environments showed that the parameters necessary for the simulation were the shroud bulk temperature caused by ascent heating, the oxygen diffusion rate to the titanium surface, and the nuclear energy disposition profile. A variable pressure wind tunnel and sample heater was designed, fabricated, and calibrated to produce the required oxygen diffusion rate to the sample surface and the proper material bulk temperature. This hardware was coupled to an electron beam machine at Physics International Company to provide a pulsed radiation source. Details of the electron beam simulation will not be given here, but are contained in a report on this project from Physics International (PI).

Prior to the test, simulation and nuclear environmental parameters were compared to determine the numerical relationship between the experiment and a projected encounter. The comparison was based on energy balance calculations which quantized the various energy loss and gain mechanisms associated with the titanium surface immediately following

either X-ray or e-beam deposition. Energy is supplied to the surface by the TiO_x reaction kinetics while convection, radiation, and conduction are all loss mechanisms. Results of these preliminary calculations showed that the simulation could be considered a factor of 10 overtest when compared to a nuclear threat. The oxygen diffusion rate to the surface was higher than flight predictions resulting in increased reaction energy and the flatter e-beam deposition profile resulted in a factor of 10 lower conduction loss than was present with X-ray deposition.

Based on the above calculations it was anticipated that the titanium surface in the experiment would exhibit a brief combustion period following electron-beam deposition which would last until the surface cooled below the 1600^{o}K ignition temperature. This behavior was observed in Hi-Cam film records of the titanium sample surface. A combustion phase lasting on the order of 100 msec following e-beam deposition was recorded. The sample bulk temperature for these preliminary experiments ranged from 294^{o} to 977^{o}K, the surface temperature following e-beam deposition was 1900^{o}K, and the oxygen diffusion rate was 7.8×10^{-2} kg/m^2 sec which was a factor of four greater than the predicted maximum value at 90 kft in the missile ascent trajectory.

The objective of the first phase of this program was to design, fabricate, and test the experimental hardware to determine if it was capable of simulating an overtest of a 90 kft nuclear encounter. The experiment was a success in that it demonstrated the simultaneous simulation of the critical encounter parameters of material bulk temperature, oxygen diffusion rate, and pulsed deposition profile. A more complete testing program is currently being planned in which the titanium samples will be subjected to a range of parameters where the deposition profile, oxygen diffusion rate, and sample bulk temperature will be varied. The objective will be to define the parameter space in which sustained combustion is possible. Other materials such as Inconel will also be tested during these later experiments.

SECTION 2

TECHNICAL DISCUSSION

2.1 SIMULATION REQUIREMENTS

Simulation parameters for the aerothermal environment of an advanced missile shroud were derived from data on the monocoque design (Figure 1) from Martin Marietta Corporation (Reference 1). The purpose of this program was to conservatively simulate an upper atmosphere nuclear encounter that might result in sustained combustion of the titanium shroud. During the ascent phase of its trajectory the shroud is heated convectively by the atmosphere. Upon exposure to a nuclear environment (Figure 2) in the upper atmosphere, the lower-energy X-rays from the burst will cause the surface scale to blow off and heat the base material leaving a fresh titanium surface at a temperature of T_{melt}, or $1900^{o}K$. Since this is above the published ignition temperature of $1600^{o}K$ for titanium, sufficient oxygen availability could cause the shroud to ignite and burn. Therefore, the relevant parameters that must be included in the simulation are (1) the titanium bulk temperature caused by ascent heating, (2) surface temperature and temperature gradient caused by the nuclear energy deposition, and (3) oxygen flux through the boundary layer to the hot titanium surface.

Predicted bulk temperatures for the monocoque design are shown in Figure 3. As expected, the leading cone achieves the highest temperature of $\approx 880^{o}K$ at 65 sec into the flight corresponding to an altitude of $\approx$90 kft. For the simulation, the maximum sample bulk temperature was $977^{o}K$ which provides a fairly mild overtest on this parameter.

Oxygen flux through the boundary layer to the hot titanium surface was calculated from convective heat transfer predictions from W. J. Maegley's

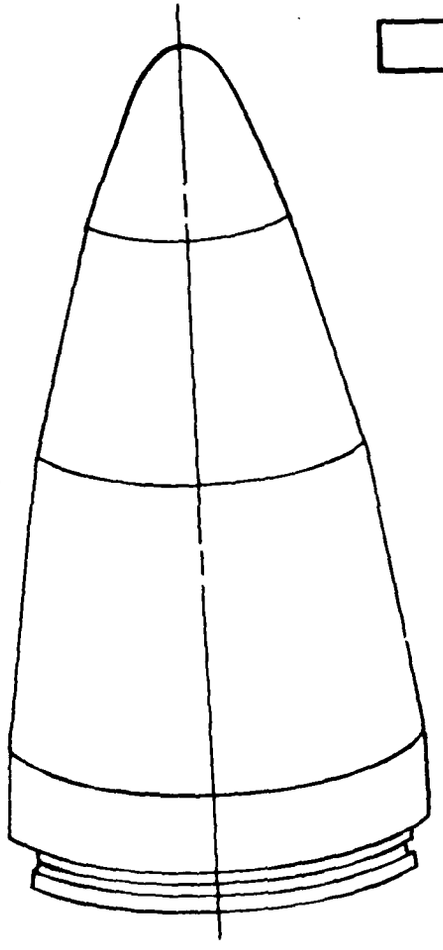

A-17403

ANGLE	THICKNESS
22.6°	2.67 mm
15.6°	1.68 mm
8.5°	2.29 mm
0°	2.29 mm

- Titanium (6 AL-4V)
- Monocoque
- 20 mm nose radius
- 4.45 m length

Figure 1. Shroud design features.

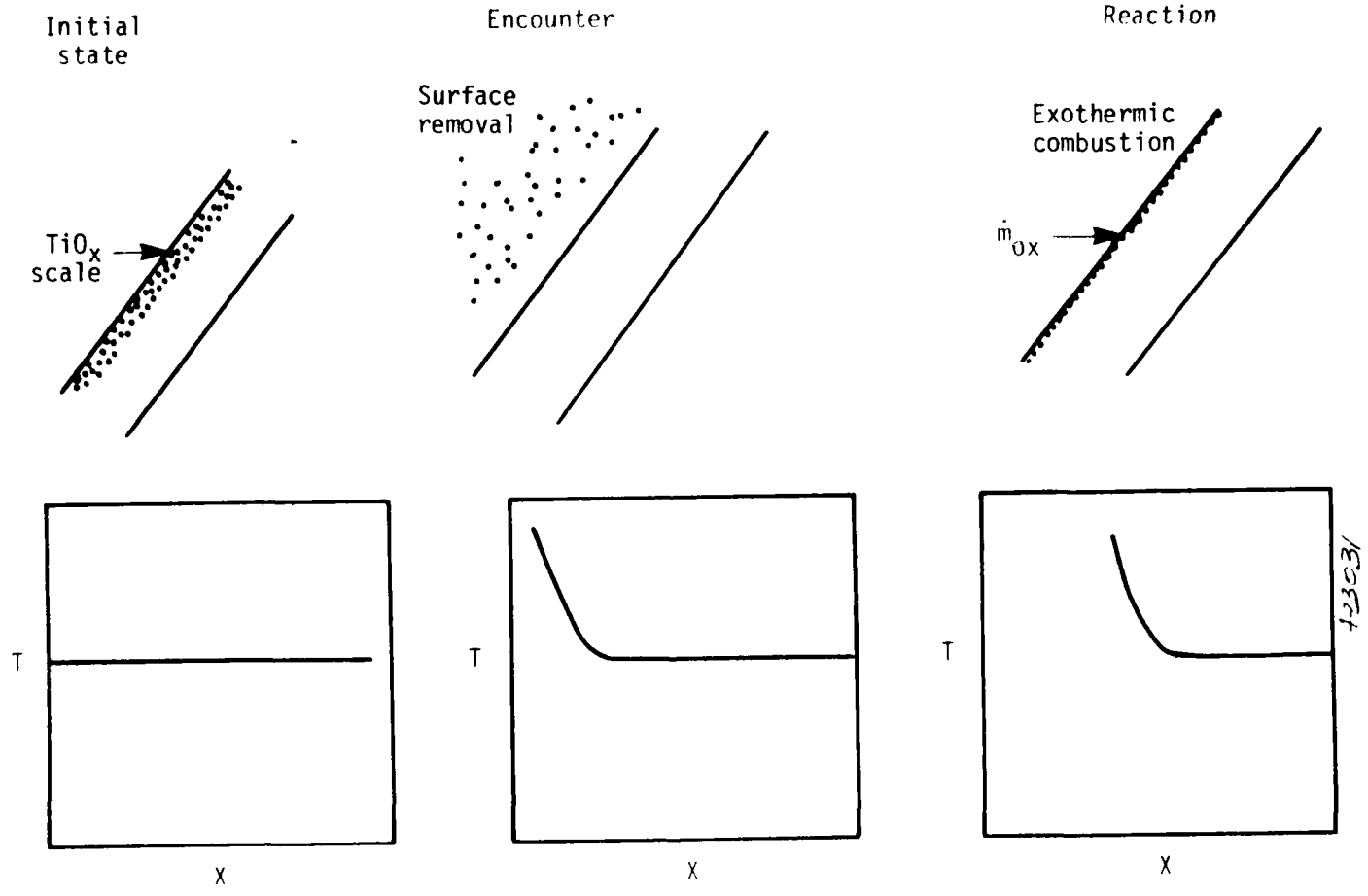

Figure 2. Titanium combustion process.

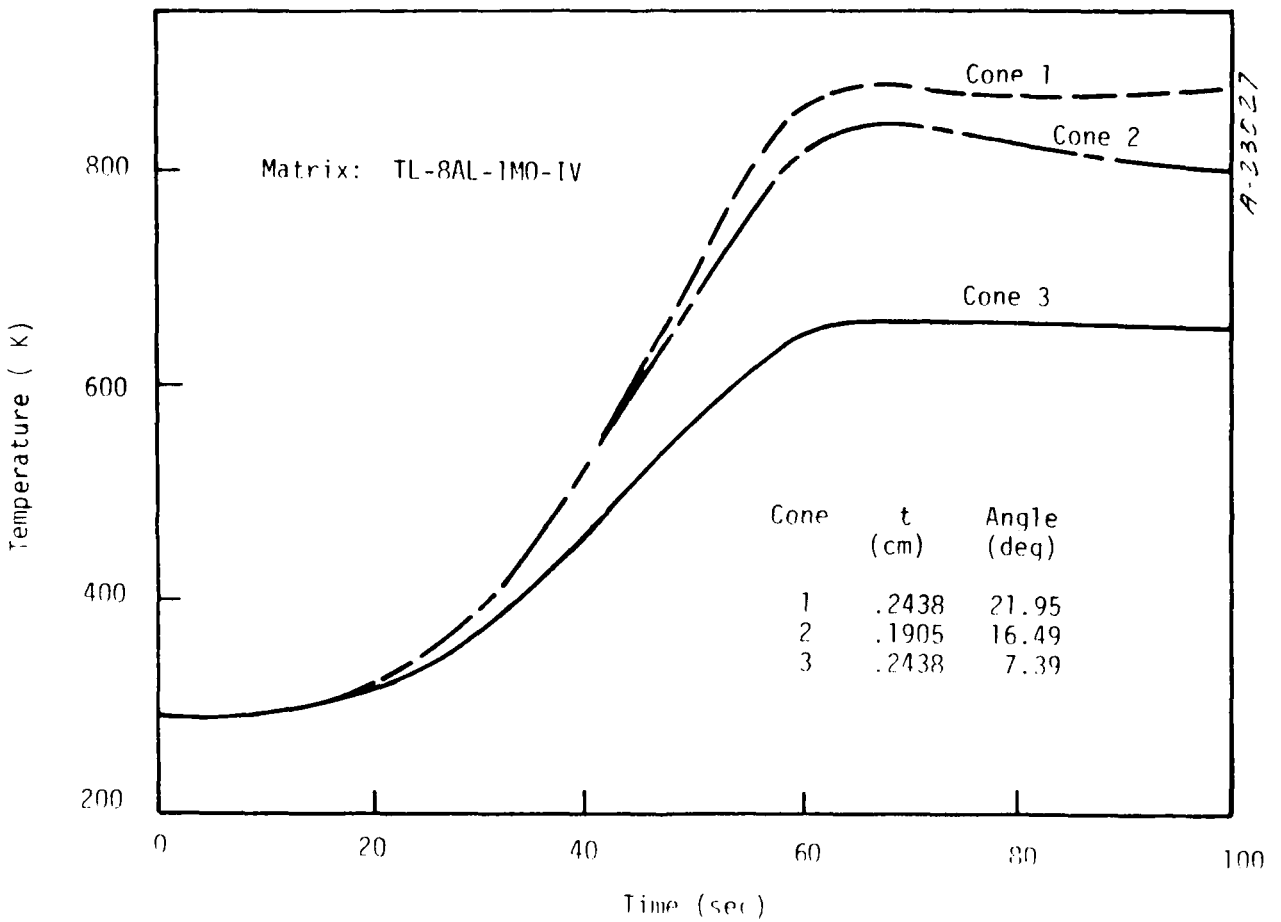

Figure 3. Shroud ascent bulk temperature history.

work.* Figure 4 illustrates the O_2 flux values calculated for a 90 kft altitude as a function of distance along the shroud. The values range from 0.2×10^{-2} kg/m^2 sec to 1.5×10^{-2} kg/m^2 sec. At the stagnation point on the shroud the oxygen flux increases to a maximum of 2.4×10^{-2} kg/m^2 sec.

2.2 HARDWARE DESIGN

To simulate the aerothermal environment described above, a wind-tunnel combined with a radiant sample heater was designed and fabricated (Figure 5). The tunnel is a blow-down design and is operated by attaching it to a vacuum source. During the experiment the tunnel was connected through a gate valve to a 7000 liter vacuum tank which was normally evacuated to a pressure of 1 torr. At the highest tunnel flowrate this vacuum tank provided a stable run time of ≈10 sec.

The wind tunnel was capable of operating over a range of inlet pressures from 10 torr to 1 atm. This operating range was required since, prior to the experiment, there was some doubt concerning the ability of the electron-beam machine to propagate a uniform beam through 1 atm of air. Air entered the wind tunnel through an aperture in a plenum chamber. By using various size apertures the ambient pressure over the sample could be varied from 10 torr to 1 atm. Figure 6 shows the predicted oxygen diffusion rate to the sample surface as a function of a plenum pressure for a flow velocity of Mach 1. These predicted values were calculated assuming laminar flow over a smooth wall and constitute a lower limit. As can be seen from the graph, these calculated O_2 rates are in the same range as the predicted flight values. The flight values of oxygen diffusion rate are dependent on cone angle of the monocoque section and axial distance along that section; therefore, they exhibit a factor of 10 difference between the stagnation point and the aft surface of the shroud.

A 6 kW array of quartz-halogen lamps were used to heat the sample to 900^{o}K prior to e-beam deposition. Sample temperature was monitored

---

*Maegley, W. J., "MX Assembly, Test, and Systems Support Data Book; MX Aerodynamic Heating Data," Martin Marietta Corporation, Denver, Colorado, report number SE0016.

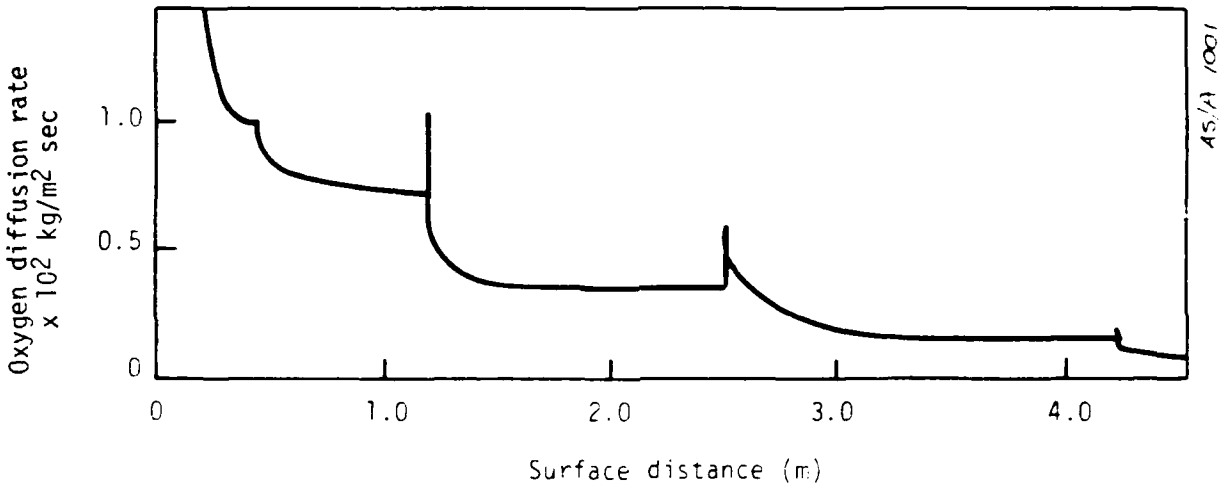

Figure 4. Oxygen diffusion rate to shroud surface for 90 kft altitude.

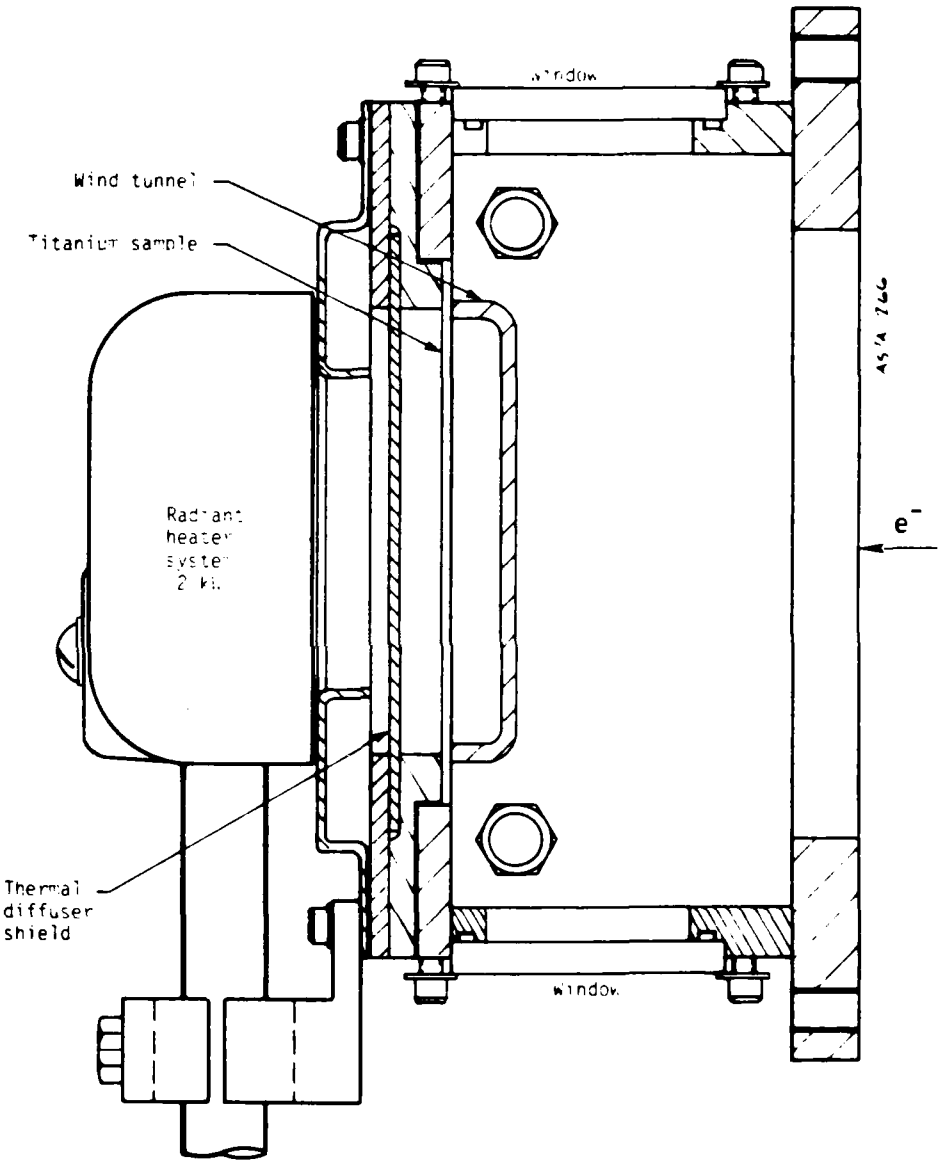

Figure 5. Wind tunnel design.

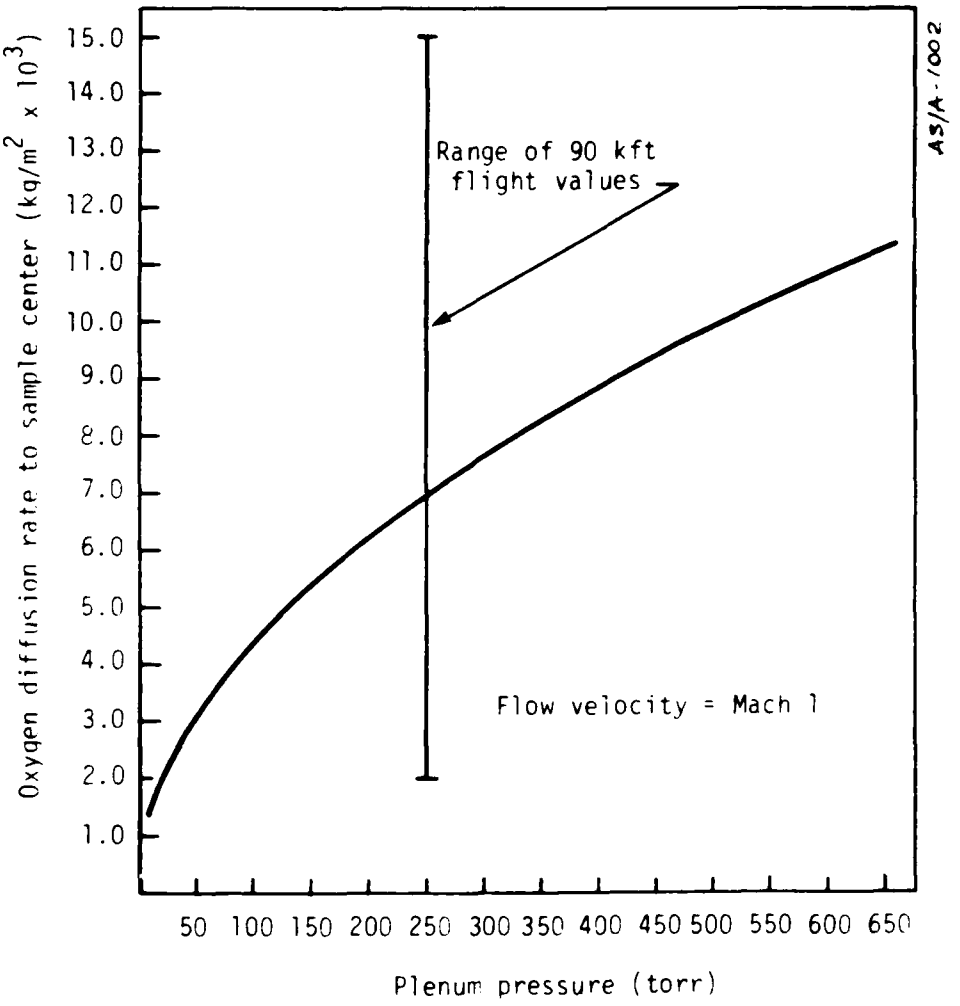

Figure 6. Predicted oxygen diffusion rate to sample surface as a function of plenum pressure.

with a sheathed thermocouple attached to the center of its rear surface. During the experiment, the sample temperature was controlled by manually cycling power to the lamps while continuously monitoring the thermocouple output. The lamp array was a water and air cooled commercially available unit from Research Incorporated, Model 5208. In the initial design, a stainless steel diffuser shield was interposed between the sample and the lamp array to diffuse the thermal flux to the sample and protect the lamps in the event of rear-surface spall. During calibration, the presence of the diffuser shield made it impossible to heat the sample to the required level of $900^{o}K$ with the available radiative flux from the lamp array. Although some rear surface spall was observed in the first few e-beam sample shots, the spall did not fully separate from the sample which indicated that the diffuser shield was not necessary. Therefore, the diffuser was removed for the experiment in an effort to get higher sample temperatures. Without the shield, the maximum achievable sample temperature exceeded $1000^{o}K$.

All wind tunnel components were fabricated from number 304 stainless steel. Windows were provided on both sides of the tunnel housing to record the sample front surface reaction with high speed movies.

2.3 WIND TUNNEL CALIBRATION

The objective of the calibration was to determine the wind tunnel flow velocity, uniformity, and plenum pressure as a function of aperture diameter. Various sized apertures could be installed in the air inlet to the plenum chamber to control the static pressure over the titanium sample. Aperture diameters ranged in size from 0.5 cm to 2.5 cm and could reduce the pressure of the air over the sample to <20 torr.

The vacuum source for the calibration tests was the Acurex steam extractor system which was capable of producing vacuums in the range of 1 torr. A 6 in. gate valve connected the wind tunnel to the vacuum source. Pressure transducers were installed in the side of the plenum chamber and also 8 cm downstream of the trailing edge of the sample in the wall of the wind tunnel. The downstream transducer recorded the reservoir pressure. Flow velocity over the sample is determined by the ratio of plenum pressure to reservoir pressure as shown in Figure 7. The highest pressure ratio achievable with this type of system is 1.89 which

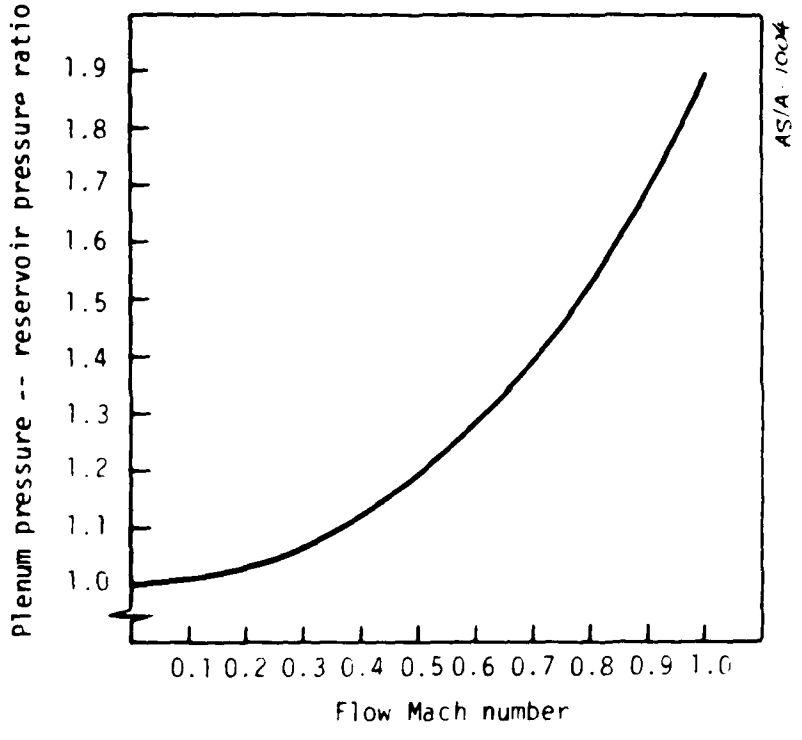

Figure 7. Wind tunnel pressure ratio as a function of flow Mach number.

corresponds to a Mach 1 flowrate in the tunnel. At this point, the flow becomes choked and no further velocity increase is possible with this design.

Figure 8 shows the results of the aperture calibration. Plenum pressures ranged from 15 torr to 250 torr for aperture diameters or from 0.5 cm to 2.5 cm. In all cases, the flow was choked as indicated by a constant ratio of 1.89 between the plenum and reservoir pressures for all aperture diameters. The most stable way to operate a wind tunnel is using this type of blow-down design since the plenum pressure and flow velocity are independent of the vacuum tank pressure as long as the ratio does not drop below the 1.89 value. Since the largest available aperture was 2.5 cm diameter, the cover was removed from the plenum chamber to go to higher pressures, thus increasing this pressure to 1 atm. For this test, the reservoir pressure was recorded at 405 torr, again indicating choked flow operation.

To check for flow uniformity over the sample surface, pitot tubes were used to scan the flow at a height of 1 cm above the sample surface in a matrix of points around the sample center. The pitot tubes had a 0.75 mm inside diameter, 1.25 mm outside diameter, and scanned the flow for a distance of 2 cm on all sides of the sample center. Results of these measurements showed that the flow was parallel to the sample and uniform at all points.

2.4 SIMULATION ANALYSIS

Relating the simulation experimental results to the anticipated material response in a nuclear threat environment requires quantitatively relating the simulation and nuclear parameters within the context of the combustion scenario. The major parameters of interest here are the material surface temperature, the energy deposition profile, and the oxygen diffusion rate to the surface.

A preliminary analysis was performed to investigate the magnitude of the combustion threat. The analysis was based on an energy balance calculation performed for the time immediately following energy deposition (nuclear or e-beam). When the energy is deposited in the titanium surface, the outermost material is blown off because of the sudden pressure rise and the vaporization of the surface generated by the in-depth deposition. The remaining surface will be at the melt

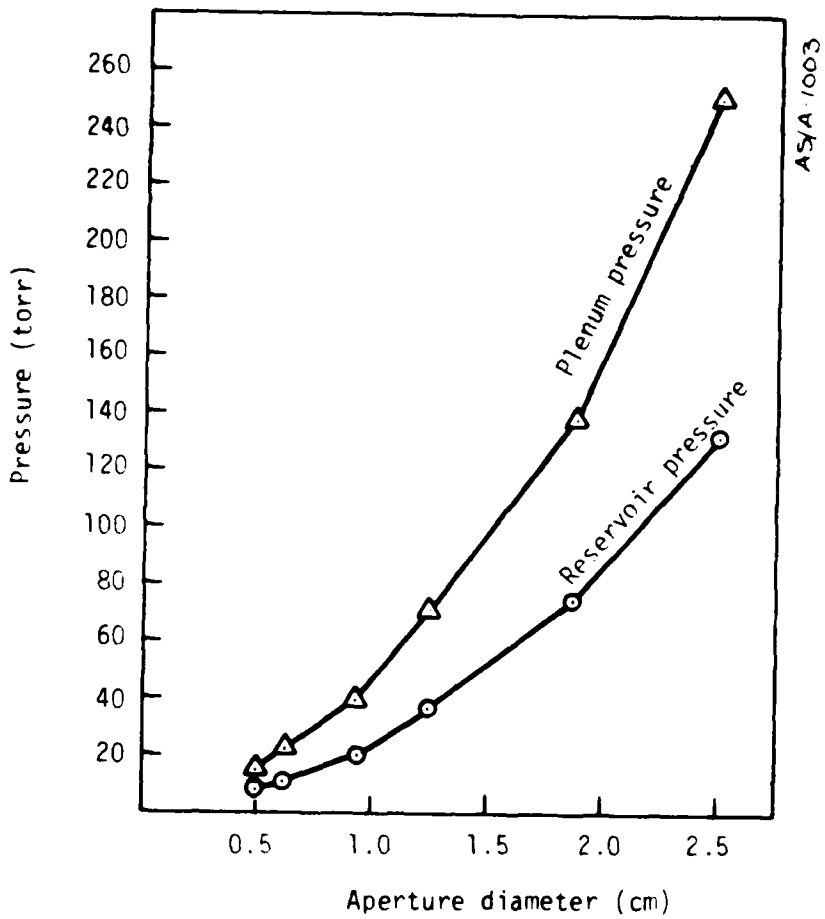

Figure 8. Wind tunnel calibration data.

temperature (1900°K for titanium). This process is the same for X-ray or e-beam deposition so the surface temperature is simulated with good fidelity. Since the 1900°K surface temperature is above the 1600°K ignition point for titanium, oxygen diffusing through the boundary layer will cause the surface to combust. The combustion reaction supplies energy to the surface at a rate directly proportional to the oxygen diffusion rate. TiO_x reaction rate kinetics were not included in this analysis since the surface reaction was not kinetically limited and the burning titanium at 1900°K could absorb several orders of magnitude more oxygen than was available.

Energy is transported away from the burning titanium surface by two primary mechanisms, radiation and conduction into the bulk of the material. Radiation loss is dependent on surface temperature and is governed by

$$Q_{rad} = \varepsilon \sigma T^4$$

where Q_{rad} is the radiated energy in watts/m^2, ε is the surface emissivity, σ is the Stefan-Baltzmann constant which equals 5.67 x 10^{-8} watts/m^2 $^oK^4$, and T is the surface temperature in ^oK. Conduction into the bulk of the material is governed by the titanium's thermal diffusivity and the surface temperature gradient. To illustrate the conduction loss mechanism, Figure 9 shows a comparison of several X-ray and e-beam deposition profiles. Because the X-ray deposition profiles have a much steeper gradient at the surface than the e-beam profiles, the conduction energy losses from the surface are an order of magnitude larger for X-ray deposition than for the e-beam. Radiative losses are the same for both cases since the surface temperature is the same for either e-beam or X-ray deposition. Convective heat transport losses are so small in comparison to conduction and radiation that they will not be considered here.

Figure 10 illustrates the heat sources and sinks following energy deposition as a function of oxygen availability, surface temperature, and surface temperature gradient. If the TiO_x reaction energy exceeds the sum of the conductive and radiative losses, the surface temperature will be rising and sustained combustion is probable. If the losses are greater

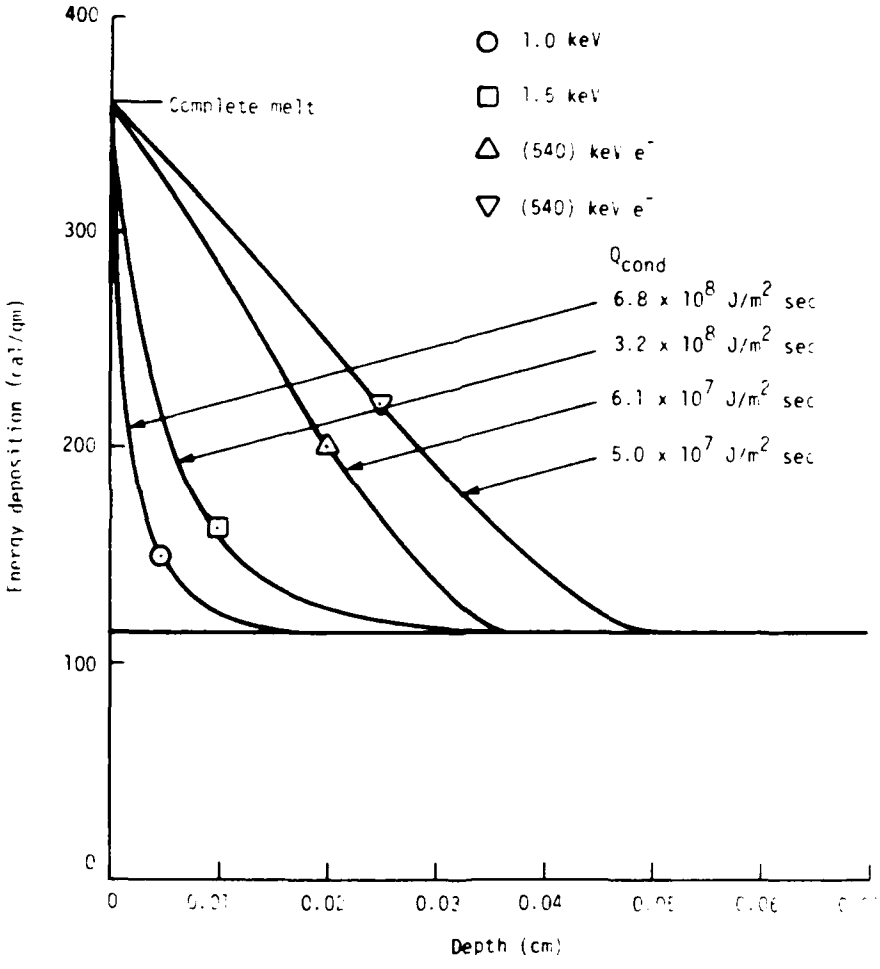

Figure 9. Comparison of e-beam and X-ray deposition profiles.

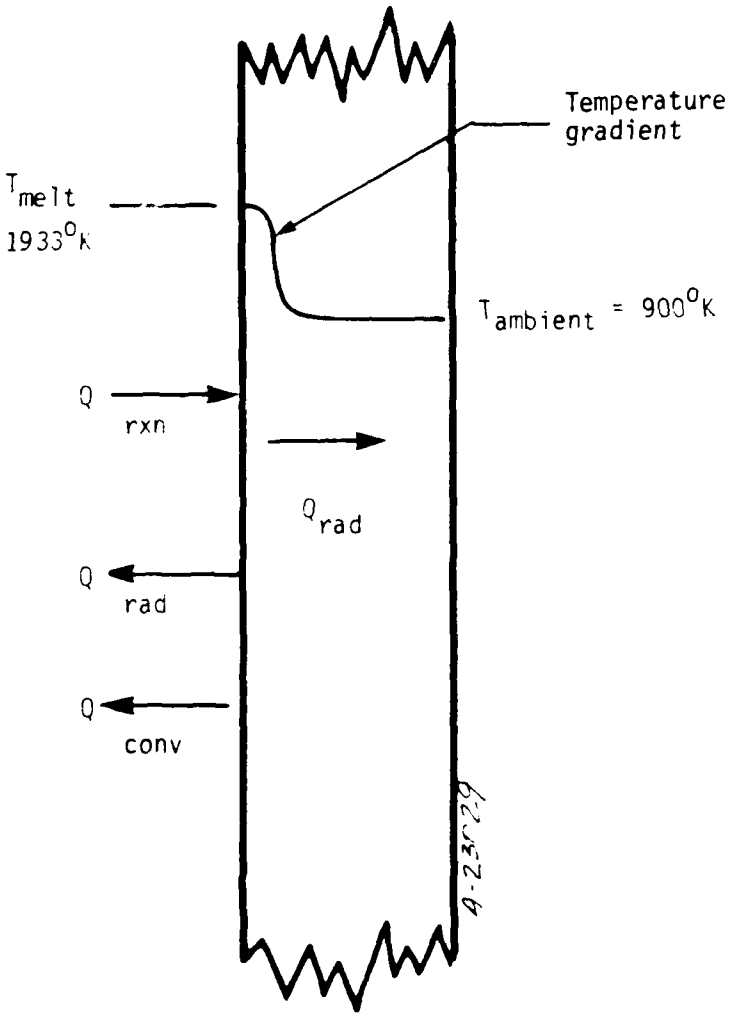

$$Q_{rxn} = Q_{cond} + Q_{conv} + Q_{rad}$$

Figure 10. Energy requirements for combustion.

than the reaction energy, the surface temperature will decrease and the combustion process will cease.

Table 1 lists the analysis parameters for both the nuclear encounter and the e-beam simulation experiment. For both cases, the bulk material temperature, surface temperature, and radiative energy loss rates are identical. The oxygen diffusion rate in the simulation is somewhat higher (Table 1) than predicted for the shroud making this a 62 percent overtest for that parameter. Conduction losses are an order of magnitude higher in the nuclear scenario than the e-beam case, making this a more severe overtest since conduction is the primary cooling mechanism for the titanium surface. In either case, however, sustained combustion is very unlikely since the reaction energy heating the surface is much less than the amount of heat being removed by conduction. The simulation experiment provides a good overtest of this situation since the conduction energy losses immediately following deposition are lower by and the oxygen transport to the surface is higher by 62 percent than the maximum predicted for a nuclear encounter in the upper atmosphere.

Table 1. Nuclear environment versus simulation parameters.

	Nuclear Threat	E-Beam Simulation
Bulk temperature	900°K	900°K
Surface temperature	1900°K	1900°K
O_2 diffusion	$\leq 4.80 \times 10^{-2}$ kg/m^2 sec	7.8×10^{-2} kg/m^2 sec
$Q_{conduction}$	$3.2 - 6.8 \times 10^{8}$ J/m^2 sec	$5.0 - 6.1 \times 10^{7}$ J/m^2 sec
$Q_{radiation}$	4.0×10^{5} J/m^2 sec	4.0×10^{5} J/m^2 sec
$Q_{reaction}$	$\leq 1.4 \times 10^{6}$ J/m^2 sec	2.2×10^{6} J/m^2 sec

SECTION 3

EXPERIMENT

A schematic of the simulation experimental configuration is shown in Figure 11. Following installation, a brief calibration check was run on the wind tunnel using the 7000 liter blow-down tank to ensure that the plenum pressures and flowrates were the same as observed in the initial calibration sequence. Tests run with the 0.5 cm and 2.5 cm apertures with the cover removed from the plenum chamber confirmed that the operating characteristics were the same with the blow-down tank as with the steam extractor vacuum system. Stable run times were longer with the blow-down tank because of its larger capacity. Operating at the maximum mass flowrate, plenum pressure of 1 atm, stable run times of 10 sec were recorded. These run times were a factor of 10 longer than any observed transient combustion times indicating that sufficient observation times were used to record the response of the titanium surface.

Wind tunnel performance was monitored with the reservoir pressure transducer located on the tunnel wall downstream from the trailing edge of the sample. Since the wind tunnel is operated in a choked flow mode (constant ratio of 0.52 between the pressures in the reservoir and the plenum chamber), this single pressure transducer was sufficient to record the tunnel performance. Titanium preheat temperature was recorded by a sheathed thermocouple mounted near the center on the back wall of the sample. All data were recorded on an oscillograph. Pressure and temperature data were also monitored in real time with digital readouts.

Preliminary electron beam shots were used to characterize the beam in terms of electron energy spectrum, fluence, and uniformity. Initial calorimeter shots taken with the wind tunnel operating at 1 atm demonstrated that the e-beam could deliver a uniform beam with sufficient

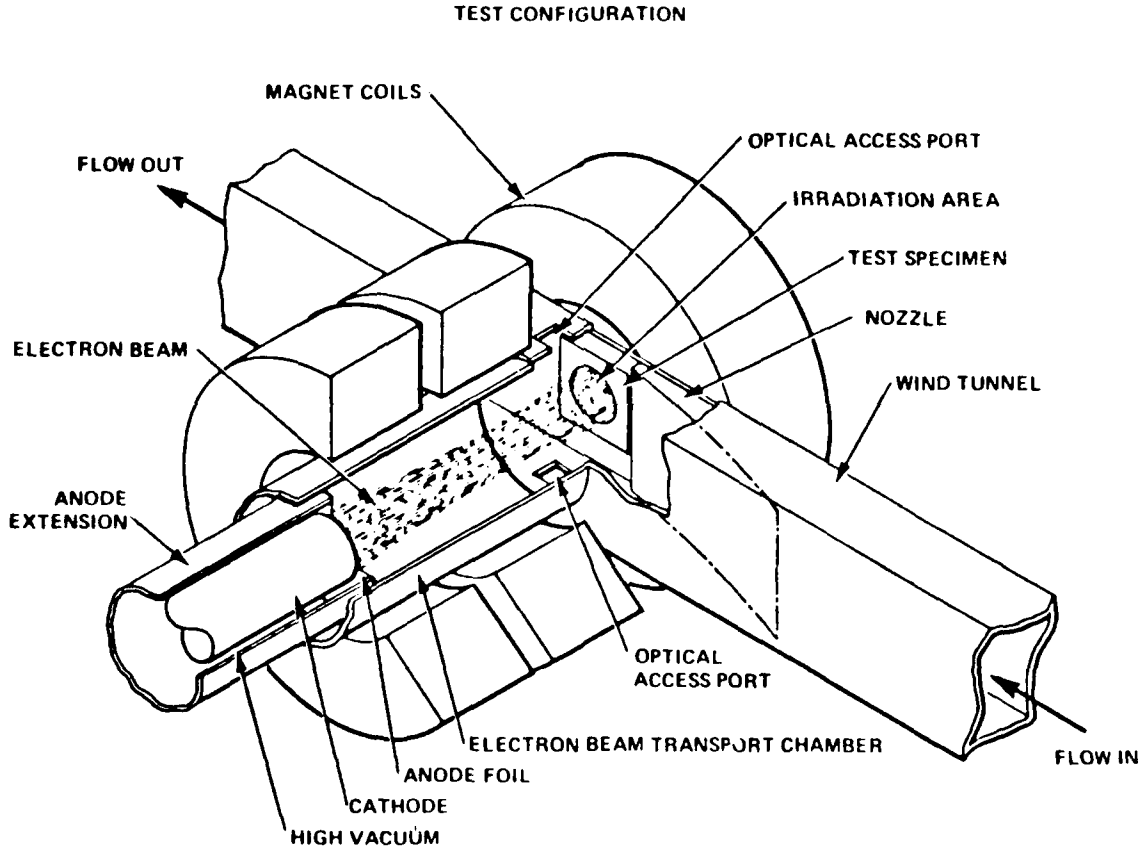

Figure 11. Simulation experimental configuration.

fluence to the target under these conditions. Therefore, all titanium samples were irradiated with the wind tunnel operating at maximum mass flowrate.

A summary of the shot matrix from these experiments is shown in Table 2. Shot number 2199 was a calorimeter shot where a segmented graphite calorimeter was mounted in the wind tunnel at the sample location. The beam was fired with the wind tunnel operating at maximum capacity. After propagating through several inches of 1 atm air, the beam exhibited good uniformity and had sufficient fluence to drive the surface of a titanium sample to $1900^{o}K$ or T_{melt}.

Shots 2200 through 2202 were taken with the sample at room temperature. Maximum airflow was used on 2200 and 2202, but no wind tunnel was used on 2201 for the sake of comparison. All three samples exhibited incipient rear surface spall and a uniform front surface crater.

The sample was heated to $622^{o}K$ for shot number 2204. Although the front-surface crater appeared uniform on the shot, the spall pattern was torroidal in shape indicating a nonuniform beam. Beam uniformity is not a particularly critical issue for this experiment. As long as the entire beam area is cratered, material will be removed down to the level of T_{melt} leaving the remaining surface at a uniform temperature.

Prior to shot 2204, the sample in the wind tunnel was subjected to a thermal cycle with and without airflow to more accurately define the oxygen diffusion rate to the surface. The sample was heated to $700^{o}K$ and allowed to begin cooling with the lamps off. At $\approx 600^{o}K$, the airflow was turned on so that the cooling rate could be measured with and without forced convection. From these cooling curves the mass transfer coefficient for the airflow which is directly proportional to the oxygen diffusion rate can be calculated. Based on these measurements, the oxygen diffusion rate to the titanium surface was 7.8×10^{-2} kg/m^2 sec for these experiments. Bulk sample temperature for shot number 2204 was $761^{o}K$.

For shot number 2208 the sample bulk temperature was increased to $811^{o}K$. The crater appeared deeper on this shot and full rear-surface spall was observed.

Shot number 2209 was the highest bulk temperature data shot at $977^{o}K$. The rear-surface spall was fully detached and driven into the

Table 2. Experimental data summary.

Shot Number	Type	Sample Temperature	$\dot{m}_{ox}$ kg/m^2 sec	Comments
2199	Calorimeter	--	7.8×10^{-2}	Good uniformity and fluence
2200	Titanium	294°K	7.8×10^{-2}	Incipient rear-surface spall. No sustained combustion.
2201	Titanium	294°K	0	Reference shot with no airflow. Incipient spall.
2202	Titanium	294°K	7.8×10^{-2}	Incipient spall but no sustained combustion
2203	Calorimeter	--	0	Good uniformity and fluence
2204	Titanium	622°K	7.8×10^{-2}	Thermocouple survived e-beam showing immediate temperature drop. Torroidal beam.
2205	Calorimeter	--	0	Better uniformity
2206	Titanium	761°K	7.8×10^{-2}	More complete spall but no sustained combustion
2207	Calorimeter	--	0	Magnet for guide field damaged
2208	Titanium	811°K	7.8×10^{-2}	Complete spall but not detached
2209	Titanium	977°K	7.8×10^{-2}	Spall destroys lamps. No sustained combustion evidence.

lamp array causing catastrophic failure of the lamps. This spall behavior was possibly because of the spall threshold being reduced by the high sample temperature.

SECTION 4

RESULTS AND CONCLUSIONS

The objective of this program was to perform an overtest simulation of an upper atmosphere nuclear encounter for titanium shroud material. This objective was achieved and the experiment was highly successful. For all system parameters, bulk temperature, surface temperature, surface temperature gradient, and oxygen diffusion rate, the simulation experiment produced equivalent or more severe conditions than would be present in a flight encounter. As predicted, none of the samples exhibited any evidence of sustained combustion. Following electron beam deposition, the titanium surface would ignite and go through a transient burn phase lasting 100 msec after which it would self-extinguish. In all cases, the airflow was left on for at least 20 sec following electron beam deposition.

The next phase of this program will be a more detailed parameter study of the nuclear encounter combustion threat using more severe environmental conditions. The objective will be to develop a methodology for predicting the response of the titanium surface and confirm the accuracy of the model through an analysis of the experimental data. This model can then be used to predict those regions of the parameter space where sustained combustion could occur. It will also provide a basis for making quantative comparisons between the simulation experiment on a predicted nuclear encounter.

DISTRIBUTION LIST

DEPARTMENT OF DEFENSE

Assistant to the Secretary of Defense
Atomic Energy
ATTN: Executive Assistant

Defense Advanced Rsch Proj Agency
ATTN: TIO

Defense Communications Agency
ATTN: CCTC

Defense Intelligence Agency
ATTN: DT-2
ATTN: DB-4D
ATTN: DT-1C

Defense Nuclear Agency
ATTN: STSP
ATTN: SPAS
ATTN: SPSS
ATTN: SPTD
4 cy ATTN: TITL

Defense Technical Information Center
12 cy ATTN: DD

Field Command
Defense Nuclear Agency
ATTN: FCTMOF
ATTN: FCTMD
ATTN: FCTMOT
ATTN: FCPR

Field Command
Defense Nuclear Agency
Livermore Division
ATTN: FCPRL

Joint Chiefs of Staff
ATTN: J-5 Nuclear Division
ATTN: SAGA/SSD
ATTN: J-5 Force Planning & Program Div
ATTN: SAGA/SFD

Joint Strat Tgt Planning Staff
ATTN: JLTW-2
ATTN: JPTM
ATTN: JLA

NATO School (SHAPE)
ATTN: U.S. Documents Officer

Under Secy of Def for Rsch & Engrg
ATTN: Engineering Technology, J. Persh
ATTN: Strategic & Space Systems (OS)

DEPARTMENT OF THE ARMY

BMD Advanced Technology Center
Department of the Army
ATTN: ATC-T, M. Capps

BMD Systems Command
Department of the Army
ATTN: BMDSC-H, N. Hurst

DEPARTMENT OF THE ARMY (Continued)

Deputy Chief of Staff for Ops & Plans
Department of the Army
ATTN: DAMO-NCZ

Deputy Chief of Staff for Rsch Dev & Acq
Department of the Army
ATTN: DAMA-CSS-N

Harry Diamond Laboratories
Department of the Army
ATTN: DELHD-N-TE
ATTN: DELHD-N-P, J. Gwaltney

U.S. Army Ballistic Research Labs
ATTN: DRDAR-BLT, R. Vitali
ATTN: DRDAR-BLE, J. Keefer
ATTN: DRDAR-BL, R. Eichelberger
ATTN: DRDAR-BLV, W. Schuman, Jr.
ATTN: DRDAR-BLT, J. Frasier
ATTN: DRDAR-BLV

U.S. Army Material & Mechanics Rsch Ctr
ATTN: DRXMR-HH, J. Dignam

U.S. Army Materiel Dev & Readiness Cmd
ATTN: DRCDE-D, L. Flynn

U.S. Army Missile Command
ATTN: DRDMI-XS
ATTN: DRSMI-RKP, W. Thomas
ATTN: DRDMI-TRR, B. Gibson

U.S. Army Nuclear & Chemical Agency
ATTN: Library

U.S. Army TRADOC Systems Analysis Activity
ATTN: ATAA-TDC, R. Benson

DEPARTMENT OF THE NAVY

Naval Research Laboratory
ATTN: Code 6770, G. Cooperstein
ATTN: Code 2627
ATTN: Code 7908, A. Williams

Naval Sea Systems Command
ATTN: SEA-0352, M. Kinna

Naval Surface Weapons Center
ATTN: Code R15, J. Petes
ATTN: Code F31
ATTN: Code K06, C. Lyons

Naval Weapons Evaluation Facility
ATTN: P. Hughes
ATTN: L. Oliver

Office of Naval Research
ATTN: Code 465

Office of the Chief of Naval Operations
ATTN: OP 604E14, R. Blaise
ATTN: OP 65
ATTN: OP 604C3, R. Piacesi

DEPARTMENT OF THE NAVY (Continued)

Strategic Systems Project Office
Department of the Navy
ATTN: NSP-272

DEPARTMENT OF THE AIR FORCE

Aeronautical Systems Division
Air Force Systems Command
2 cy ATTN: ASD/ENFTV, D. Ward

Air Force Flight Dynamics Laboratory
ATTN: FXG

Air Force Geophysics Laboratory
ATTN: LY, C. Touart

Air Force Materials Laboratory
ATTN: MBC, D. Schmidt
ATTN: MBE, G. Schmitt
ATTN: LLM, T. Nicholas

Air Force Rocket Propulsion Laboratory
ATTN: LKCP, G. Beale

Air Force Systems Command
ATTN: SOSS
ATTN: XRTO

Headquarters Space Division/YL
Air Force Systems Command
ATTN: AFML, G. Kirshner

Air Force Weapons Laboratory
Air Force Systems Command
ATTN: DYS
ATTN: DYV
ATTN: DYV, A. Sharp
ATTN: DYT
ATTN: SUL
ATTN: HO, W. Minge
2 cy ATTN: NTO

Arnold Engineering Development Center
Air Force Systems Command
ATTN: Library Documents

Ballistic Missile Office
Air Force Systems Command
ATTN: MNNR
2 cy ATTN: MNNH, Capt Blankinship

Deputy Chief of Staff
Operations Plans and Readiness
Department of the Air Force
ATTN: AFXOOSS

Deputy Chief of Staff
Research, Development & Acq
Department of the Air Force
ATTN: AFRD
ATTN: AFRDQSM

DEPARTMENT OF THE AIR FORCE (Continued)

Foreign Technology Division
Air Force Systems Command
ATTN: TQTD
ATTN: SDBS, J. Pumphrey
ATTN: SDBG

Headquarters Space Division
Air Force Systems Command
ATTN: DYS
ATTN: RSS
ATTN: RST
ATTN: RSSE

Strategic Air Command
Department of the Air Force
ATTN: DOXT
ATTN: XPFS
ATTN: XPQM
ATTN: XOBM

DEPARTMENT OF ENERGY

Department of Energy
ATTN: OMA/RD&T

DEPARTMENT OF ENERGY CONTRACTORS

Lawrence Livermore National Laboratory
ATTN: L-125, J. Keller
ATTN: L-92, C. Taylor
ATTN: L-262, J. Knox
ATTN: L-24, G. Staihle

Los Alamos National Scientific Laboratory
ATTN: J. Taylor
ATTN: J. McQueen
ATTN: R. Thurston
ATTN: R. Skaggs
ATTN: R. Dingus

DEPARTMENT OF DEFENSE CONTRACTORS

Acurex Corp
ATTN: C. Nardo
ATTN: R. Rindal
5 cy ATTN: K. Triebes

Aerojet Solid Propulsion Co
ATTN: R. Steele

Aerospace Corp
ATTN: W. Barry
ATTN: H. Blaes
ATTN: J. McClelland

Analytic Services, Inc
ATTN: J. Selig

APTEK
ATTN: T. Meagher

DEPARTMENT OF DEFENSE CONTRACTORS (Continued)

AVCO Research & Systems Group
ATTN: J. Gilmore
ATTN: Document Control
ATTN: J. Stevens
ATTN: W. Broding
2 cy ATTN: P. Grady

Boeing Co
ATTN: B. Lempriere
ATTN: R. Holmes

California Research & Technology, Inc
ATTN: K. Kreyenhagen

Calspan Corp
ATTN: M. Holden

Effects Technology, Inc
ATTN: R. Wengler
ATTN: R. Parisse
ATTN: M. Rosen

General Electric Co
Space Division
ATTN: G. Harrison
ATTN: C. Anderson
ATTN: D. Edelman

General Electric Co
Re-Entry & Environmental Systems Div
ATTN: P. Cline

General Electric Company—TEMPO
ATTN: DASIAC

Hercules, Inc
ATTN: P. McAllister

Institute for Defense Analyses
ATTN: J. Bengston
ATTN: Classified Library

Kaman Sciences Corp
ATTN: J. Keith
ATTN: D. Sachs
ATTN: F. Shelton

Lockheed Missiles & Space Co, Inc
ATTN: F. Borgardt

Lockheed Missiles & Space Co, Inc
ATTN: R. Walz

Martin Marietta Corp
ATTN: E. Strauss

McDonnell Douglas Corp
ATTN: H. Berkowitz
ATTN: L. Cohen
ATTN: E. Fitzgerald
ATTN: R. Reck

DEPARTMENT OF DEFENSE CONTRACTORS (Continued)

National Academy of Sciences
National Materials Advisory Board
ATTN: D. Groves

Northrop Corp
ATTN: D. Hicks

Pacific-Sierra Research Corp
ATTN: G. Lang
ATTN: H. Brode

Physics International Co
ATTN: J. Shea
2 cy ATTN: R. Peterson

Prototype Development Associates, Inc
ATTN: J. McDonald
ATTN: J. Dunn

R & D Associates
ATTN: F. Field
ATTN: P. Rausch
ATTN: W. Graham, Jr.
ATTN: C. MacDonald
ATTN: J. Carpenter
ATTN: P. Haas

Rand Corp
ATTN: J. Mate

Rockwell International Corp
Rocketdyne Division
ATTN: G. Perrone

Science Applications, Inc
ATTN: D. Hove
ATTN: O. Nance
ATTN: W. Yengst
ATTN: J. Warner
ATTN: G. Ray

Science Applications, Inc
ATTN: G. Burghart

Science Applications, Inc
ATTN: W. Layson
ATTN: J. Cockayne

Science Applications, Inc
ATTN: A. Martellucci

SRI International
ATTN: D. Curran
ATTN: G. Abrahamson
ATTN: H. Lindberg
ATTN: P. Dolan

System Planning Corp
ATTN: F. Adelman

Systems, Science & Software, Inc
ATTN: R. Duff
ATTN: G. Gurtman

DEPARTMENT OF DEFENSE CONTRACTORS (Continued)

TRW Defense & Space Sys Group
ATTN: D. Baer
ATTN: W. Wood
ATTN: P. Brandt
ATTN: G. Arenguren
ATTN: A. Zimmerman
ATTN: R. Bacharach
ATTN: T. Mazzola
ATTN: M. Seizew

DEPARTMENT OF DEFENSE CONTRACTORS (Continued)

TRW Defense & Space Sys Group
ATTN: V. Blankenship
ATTN: I. Berger
2 cy ATTN: W. Polich

Thiokol Corp
ATTN: W. Shoun